

Comparison of single-channel and multichannel aerosol optical depths derived from MAPSS data

Istvan Laszlo,^{1,3} Hongqing Liu,² and Alexander Ignatov¹

Received 1 December 2007; revised 7 July 2008; accepted 17 July 2008; published 10 October 2008.

[1] Previous comparisons of the single-channel and multichannel aerosol products reported in the Clouds and the Earth's Radiant Energy System (CERES) Single Scanner Footprint (SSF) data sets showed systematic differences that were partly attributed to differences in sampling and cloud screening. This study concentrates on quantifying the aerosol optical depth (AOD) differences when the above differences are absent and exactly the same clear radiances are inputted to the aerosol algorithms used to generate the two products. This is accomplished by retrieving AOD with the single-channel algorithm at 22 oceanic locations from the reflectance data in the Moderate Resolution Imaging Spectroradiometer (MODIS) Atmosphere Parameters Subset Statistics (MAPSS) data set for the period of 2000–2007 and then by comparing them to the corresponding MODIS AOD data reported in MAPSS. Comparisons of AODs are performed for two MODIS instruments flown onboard the Terra and Aqua platforms at two wavelengths. On average, the mean differences are wavelength and platform dependent. The single-channel 644-nm AODs are larger by 0.004–0.015 (~2–9%) than those from the multichannel algorithm. The mean AOD at 1632 nm from both algorithms are very similar from Terra, but the single-channel AOD from Aqua at 2119 nm is lower by 0.02 (~24%). The mean absolute differences are 0.022–0.025 and do not change much with wavelength or platform. Slight dependence of the mean differences on the scattering angle is observed, which is partially explained by the differences between the retrieved aerosol model in the multichannel retrieval and the fixed aerosol model used in the single-channel algorithm.

Citation: Laszlo, I., H. Liu, and A. Ignatov (2008), Comparison of single-channel and multichannel aerosol optical depths derived from MAPSS data, *J. Geophys. Res.*, 113, D19S90, doi:10.1029/2007JD009664.

1. Introduction

[2] Several satellite-derived aerosol products over ocean are available today for studying the effect of aerosols on radiation and climate. They are derived from different satellite-measured radiances employing different retrieval techniques. The complexity of the algorithms vary from simple single-channel retrievals that assume a fixed aerosol model and estimate only the column amount of aerosol from radiances in a single-channel to complex multichannel and multiangle algorithms that use a number of representative aerosol models and retrieve the amount and some other characteristic of the aerosol (e.g., particle size, most likely aerosol model, fraction of fine-mode aerosol) simultaneously from radiances in two or more channels. Other algorithms combine multispectral and multiangle measurements with polarized radiance measurements (e.g., the algorithms used

with the Polarization and Directionality of the Earth's Reflectances (POLDER) instrument [Deuze *et al.*, 2000] or with the upcoming Aerosol Polarimetry Sensor (APS) [Mishchenko *et al.*, 2007]). An example of the single-channel algorithms is the algorithm developed at the National Oceanic and Atmospheric Administration (NOAA), National Environmental Satellite, Data, and Information Service (NESDIS) and used for routine retrieval of aerosol optical depth (AOD) from the short-wavelength channel (0.63, 0.86 and 1.6 μm) measurements of the Advanced Very High Resolution Radiometer (AVHRR) [Stowe *et al.*, 1997, 2002; Ignatov *et al.*, 2004]. The algorithms developed at the National Aeronautics and Space Administration (NASA) and used with multispectral radiances from the Moderate Resolution Imaging Spectroradiometer (MODIS) [Tanré *et al.*, 2001; Levy *et al.*, 2005; Remer *et al.*, 2005] and from the Multiangle Imaging Spectroradiometer (MISR) [e.g., Diner *et al.*, 1998; Kahn *et al.*, 2001] represent the most complex algorithms to date.

[3] It is not uncommon to see different algorithms being applied to radiances derived from the same satellite instrument. For example, Ignatov *et al.* [2004] use the NESDIS single-channel algorithm, while Mishchenko *et al.* [1999] and Higurashi and Nakajima [1999] apply two-channel

¹Center for Satellite Applications and Research, NESDIS, NOAA, Camp Springs, Maryland, USA.

²PSGS/QSS Group Incorporated, Lanham, Maryland, USA.

³Also at Department of Atmospheric and Oceanic Science, University of Maryland, College Park, Maryland, USA.

algorithms to AVHRR radiances. Inputs may also differ, even from the same instrument because of different sampling including different identification of clear pixels (e.g., cloud and glint screening) thus leading to different AODs. This was also pointed out, for example, by *Myhre et al.* [2004, 2005] who intercompared monthly mean AOD over-ocean derived from nine aerosol algorithms. The algorithms included in their study ranged, among others, from simple single-channel algorithms applied to AVHRR and the Visible and Infrared Scanner (VIRS) to sophisticated multichannel algorithms employed with radiance measurements from MODIS and MISR. They found that the respective AODs were substantially different, and attributed part of the differences in AOD to differences in cloud screenings.

[4] *Kahn et al.* [2007], in a recent analysis of MODIS and MISR AOD differences over dark water, also identified cloud screening as one of the contributors to the AOD differences in addition to instrument calibration, sampling differences, and algorithm assumptions. Differences in cloud screening introduce different levels of cloud contamination in the aerosol retrievals. Cloud contamination of pixels used for aerosol retrieval is a major issue, and generally leads to a high AOD bias. For example, analyzing 1 year of MODIS AOD data, *Zhang and Reid* [2006] found 12% increase of AOD largely due to cloud-related artifacts. The contamination-induced AOD increase was even larger (30%) over the Southern Hemisphere midlatitude oceans. *Zhang and Reid* [2006] also noted that MODIS AOD retrieval is strongly affected by wind speed and aerosol microphysical properties.

[5] The Clouds and the Earth's Radiant Energy System (CERES) [*Wielicki et al.*, 1996] Single Scanner Footprint (SSF) data sets [*Geier et al.*, 2003] were the first to report two AOD products over ocean. Both are derived from MODIS radiances but use different selection of pixels and different retrieval algorithms [*Ignatov et al.*, 2005]. One aerosol product is derived from the standard 10-km multichannel MODIS aerosol products (termed MOD04 and MYD04 for the Terra and Aqua satellites, respectively) by subsetting and remapping the MODIS AOD retrievals onto the ~20-km CERES footprint. The other aerosol product is derived by applying the NESDIS single-channel algorithm to the cloud-free MODIS radiances identified by the CERES cloud mask [*Minnis et al.*, 1999] and averaged to the CERES-footprint. Even though their source is the same, the clear reflectances used in the two aerosol retrievals differ because of differences in the respective cloud masks.

[6] Several comparisons of the two aerosol products in the CERES-SSF data were made in the past. *Ignatov et al.* [2005] analyzed two weeks of SSF aerosol data from Terra and found that the two products disagreed mostly because of differences in cloud and sun-glint screening. *Ignatov et al.* [2006, Table 3] confirmed this finding and reported an overestimate in the 644-nm single-channel aerosol optical depth by 0.011 and 0.013, respectively from Terra and Aqua. *Zhao et al.* [2005a, 2005b] examined an entire year of Terra CERES-SSF aerosol data and concluded that the two aerosol products were very similar; the global annual mean of 644-nm single-channel aerosol optical depth was only 0.009 higher than the multichannel one when only the highest-quality clear CERES pixels were considered. Both analyses were global, but they used different time periods

and different versions of the SSF data. The numbers above are only meant to give a flavor of the differences between the two products when differences in aerosol algorithm, sampling, and algorithm versions are included. *Zhao et al.* [2005a, 2005b] and *Ignatov et al.* [2006] also noted that as the ambient cloudiness increased, the two AODs diverged progressively more, while the difference between the two respective size parameters decreased.

[7] The current study also compares single-channel and multichannel AODs, but it does not use the CERES SSF data. Instead, it compares AODs derived from identical reflectances and thus ensures the differences are only due to the retrieval algorithms and not influenced by cloud-screening and sampling differences. The approach and data used are first described, followed by the presentation of results and discussion of possible sources that contribute to the observed differences.

2. Comparison Strategy and Data

[8] To eliminate the effects of sampling differences identical reflectances should be consistently used as input to both aerosol algorithms. Because of the complexity of the preprocessing applied to the MODIS reflectances in both the CERES SSF and the MOD04/MYD04 production, it is not feasible to make the reflectances identical. Therefore an alternative method was chosen, and thus this study did not use the CERES SSF aerosol processing. Instead, the multichannel AODs and the corresponding reflectances were taken from the MODIS Atmosphere Parameters Subset Statistics (MAPSS) data set [*Ichoku et al.*, 2002]. The reflectances then were used in an off-line version of the single-channel algorithm (appropriately modified to accommodate the MAPSS reflectances) to retrieve the single-channel AODs. This process guaranteed that the reflectances used to derive the AOD in both algorithms were identical.

2.1. MAPSS Data Set

[9] The MAPSS data set has been created to help the evaluation of MODIS products and to provide a means for intercomparison and cross validation with other products [*Ichoku et al.*, 2002]. MAPSS has spatial statistics of MODIS retrievals for a 5 by 5 array of 10-km pixels centered at selected locations around the globe. Among others, the statistics include the AOD at the central pixel, the reflectance used in the retrieval of AOD of the 10-km central pixel, average of the 10-km reflectances with AOD retrievals in the 5×5 box, the average AOD for the box, and the fine-mode weight. The fine-mode weight estimated by the multichannel algorithm represents the fraction of fine-mode aerosols contributing to the total aerosol optical depth (at 550 nm). A fine-mode weight value of unity indicates small (fine mode: effective particles radius 0.10–0.25 μm) particles, while a value of zero corresponds to large (coarse mode: effective radius 0.98–2.50 μm) particles [*Remer et al.*, 2005]. These statistical parameters are calculated for most of the MOD04 (Terra) and MYD04 (Aqua) products on a regular basis.

[10] From the many sites in the MAPSS data 22 were selected. The primary source for the selection of sites was the MAPSS location list labeled “ocean.” This list had sites

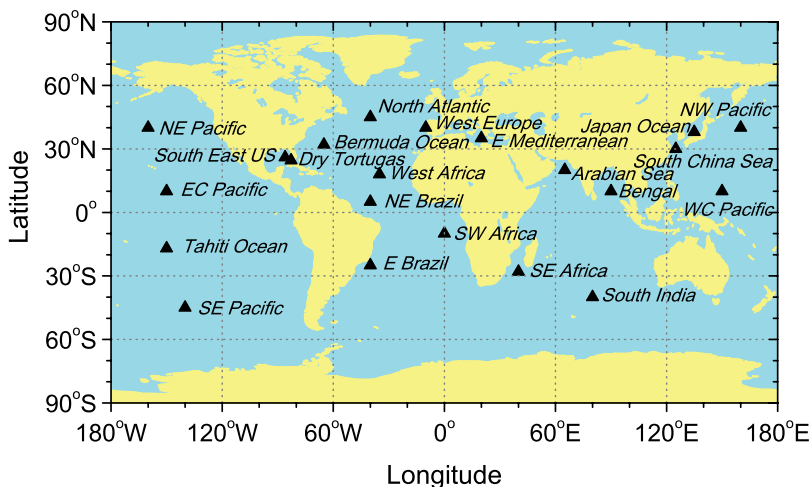


Figure 1. Geographical locations of the 22 oceanic Moderate Resolution Imaging Spectroradiometer (MODIS) Atmosphere Parameters Subset Statistics (MAPSS) sites used in the current work.

with latitudes between 47S and 45N. Out of the “ocean” sites, those away from continental coasts were chosen. A few sites not labeled “ocean” in MAPSS but commonly used in analysis of aerosol optical depth (e.g., Dry Tortugas) were added to this selection resulting in 22 sites. The geographical location of the sites is shown in Figure 1. Since the objective was to compare the satellite AOD products with each other, the selection was not restricted to AERONET sites at this time. In fact, out of the 22 locations only one (Dry Tortugas) has Sun photometer measurements. The sites represent different dominant aerosol types including oceanic aerosol over the central Pacific Ocean, dust/smoke over the middle Atlantic Ocean, smoke and some dust at South Atlantic, pollution/dust at North India, mixed aerosol at the Mediterranean and the Asian Pacific.

[11] The statistics reported in MAPSS were obtained from AODs retrieved with different versions of the MODIS aerosol algorithm (called Collections). The current study used data from Collection 5 only. At the time this study was conducted, 31 months of Terra and 34 months of Aqua Collection 5 data were available in MAPSS covering the time period of February 2000 to June 2007 for Terra and July 2002 to June 2007 for Aqua. The total number of observations used in the study was further restricted by the angular selection criteria applied (see section 2.2). In addition to the angular selection, the number of aerosol retrievals performed at the individual sites was determined by local conditions (primarily cloudiness). Out of the 22 sites, 21 sites had at least 50 retrievals for Terra and 30 for Aqua. The exception was the NW Pacific site with only 20 retrievals for Terra and 10 retrievals for Aqua. The largest number of retrievals (160) was available at the East Mediterranean and South East Africa sites. On average, the former site is dominated by fine-mode particles as suggested by the MODIS fine-mode weight (0.8 for Terra and 0.7–0.9 for Aqua), while the latter site has a mixture of fine-mode and coarse-mode particles with a dominant fine-mode weight of about 0.5–0.7 for Terra and 0.4–0.6 for Aqua. As a result of the selections due to the above angular and local meteorological constraints the sites used in this study enter with unequal statistical weights in the analysis.

2.2. Single-Channel and Multichannel Aerosol Algorithms

[12] The two aerosol algorithms compared here were described in detail by *Remer et al.* [2005] and *Ignatov et al.* [2005, 2006] therefore only their main features are reviewed in this section.

[13] The multichannel aerosol optical depth data used in this work are directly taken from the MAPSS data set. These AODs were obtained from the standard MODIS algorithm [*Remer et al.*, 2005]. The MODIS algorithm uses top-of-atmosphere (TOA) reflectances in six bands (only five for Aqua) to retrieve the optical depth, contribution of fine-mode aerosol to the total optical depth and the effective radius of aerosol particles over ocean. The retrieval uses lookup tables (LUT) of TOA reflectances calculated with the radiative transfer model of *Ahmad and Fraser* [1982] for four fine modes and five coarse modes in an atmosphere free of gas absorption. Contribution of the ocean surface is calculated from a rough ocean model with wind speed of 6 m/s. The retrieval of the above three parameters is done using all six (five for Aqua) channels simultaneously by adjusting the amount of aerosol and by selecting combinations of fine and coarse modes that best fit the observed channel reflectances.

[14] The single-channel algorithm [*Ignatov et al.*, 2004] also uses LUT for the inversion, calculated with the radiative transfer model of *Vermote et al.* [1997]. However, it does the inversion using only a single channel at a time, and thus it estimates only AOD. For this, the algorithm employs a fixed monomodal aerosol model, in contrast to the dynamically selected models in the multichannel algorithm. Similarly to the multichannel algorithm, the contribution of ocean surface is calculated from a model, but with a wind speed of 1 m/s.

[15] The MAPSS reflectances are obtained from the MOD04 and MYD04 products. These reflectances have already been “corrected” for gaseous absorption and they are used in the MODIS multichannel retrieval with lookup tables that were calculated for atmospheres free of gaseous absorption. In the CERES-SSF processing the uncorrected MODIS reflectances are used with the single-channel algo-

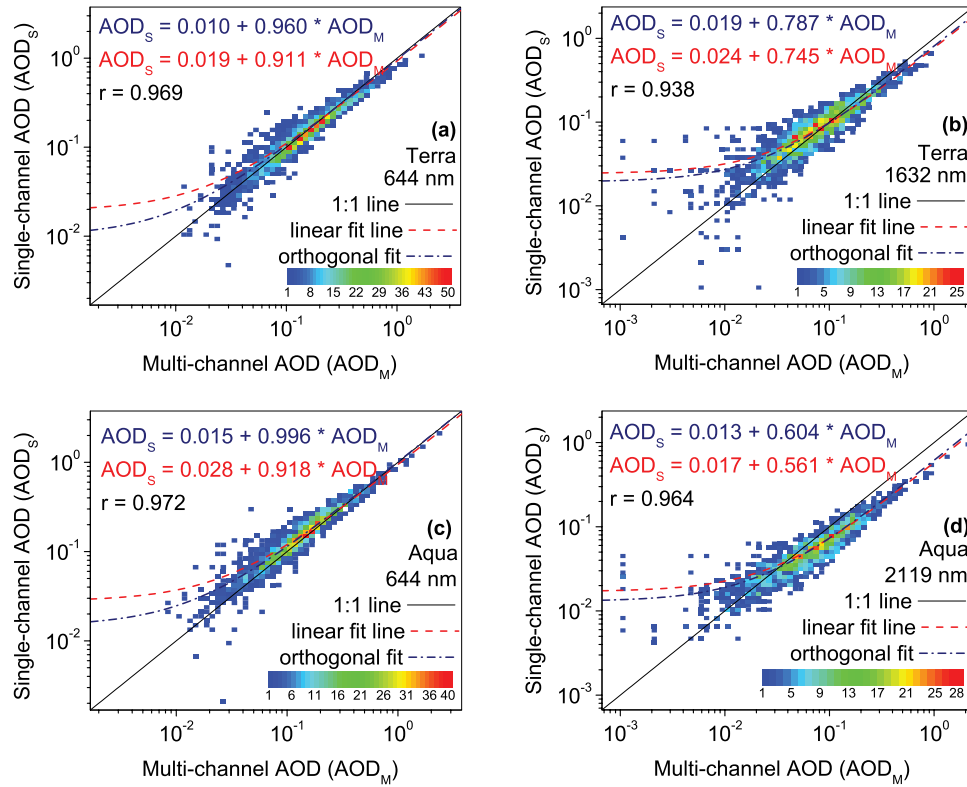


Figure 2. Scatterplots of the single-channel aerosol optical depth (AOD_S) versus the multichannel aerosol optical depth (AOD_M) for the short (a, c) and long (b, d) wavelength channels for Terra (Figures 2a and 2b) and Aqua (Figures 2c and 2d). (Note that although the results are plotted in log-log scale, the regression analyses and corresponding statistics were calculated in the linear scale.) AOD_S was retrieved from the 10-km central pixel reflectance in MAPSS, while AOD_M was obtained directly from MAPSS for the corresponding pixel. The correlation coefficient (r), the 1:1 line, and the line and coefficients of the standard and orthogonal linear fits are also shown. The scale represents the number of AOD values.

rithm and thus the original single-channel lookup tables include the absorption by gases. To be consistent with the MAPSS reflectances, the single-channel lookup tables were recalculated to exclude gaseous absorption. This makes the comparison more robust since differences due to the different treatment of gaseous absorption are avoided. In both algorithms, the LUT include the reflection by the ocean surface, multiple scattering by molecules and aerosols, absorption by aerosols (only in the multichannel algorithm). Details of the differences in the radiative transfer calculations are provided by Ignatov *et al.* [2005, Table 1] and not repeated here.

[16] The single-channel retrievals and comparisons of AODs were done at two wavelengths: 644 and 1632 nm from Terra, and 644 and 2119 nm from Aqua. (The 1632 nm MODIS channel on Aqua failed early in the mission and was replaced with the 2119 nm in this study.) AODs for glint angles $>40^\circ$, solar zenith angles $<70^\circ$, view zenith angles $<60^\circ$, and all azimuth angles were selected from the MAPSS data and single-channel AODs were retrieved from the corresponding MAPSS reflectances. Although AODs were retrieved on both sides of the satellite orbit, the current study analyzed AOD from the antisolar side only (relative azimuth angle $>90^\circ$). This was done to be consistent with the single-channel retrievals in the CERES-SSF processing

and in the comparisons by Ignatov *et al.* [2005, 2006] and by Zhao *et al.* [2005a, 2005b].

[17] The single-channel retrievals and comparisons were performed for both the central 10-km pixel and the 50-km average reflectances in MAPSS. The latter is intended to more closely simulate the CERES SSF aerosol products in the sense that the 50-km single-channel AOD is obtained from the box-average reflectance, while the multichannel 50-km AOD is the average of the 10-km aerosol optical depths.

3. Results and Discussions

[18] In this section comparisons of AOD derived from the single-channel and multichannel algorithms are presented. An attempt is also made to understand the observed differences. Because the only differences present in the retrievals are those due to the algorithms only, these differences are examined to explain the differences in AOD.

[19] In Figure 2, the single-channel AOD is plotted against the multichannel AOD from the 10-km central pixels in the MAPSS. The four panels in Figure 2 show the scatterplots for the short (644 nm) and long wavelengths (1632/2119 nm) for Terra and Aqua.

[20] The points are relatively tightly distributed along the line representing perfect agreement (one-to-one line). The

Table 1. Results of Linear Regression for Three Types of Fits^a

Wavelength (nm)	Linear fit type	a	b	σ_a	σ_b
<i>Terra</i>					
644	Standard	0.019	0.911	0.001	0.005
	Least absolute deviation	0.008	0.941		
	Orthogonal with estimated errors in both x and y	0.010	0.960	0.003	0.016
1632	Standard	0.024	0.745	0.001	0.006
	Least absolute deviation	0.018	0.776		
	Orthogonal with estimated errors in both x and y	0.019	0.787	0.002	0.020
<i>Aqua</i>					
644	Standard	0.028	0.918	0.001	0.006
	Least absolute deviation	0.013	0.976		
	Orthogonal with estimated errors in both x and y	0.015	0.996	0.003	0.019
2119	Standard	0.017	0.560	0.001	0.004
	Least absolute deviation	0.012	0.611		
	Orthogonal with estimated errors in both x and y	0.013	0.604	0.002	0.021

^aThe fit parameters offset (a) and slope (b), and their standard errors (σ_a , σ_b) are shown. Linear Regression is given by $AOD_S = a + b AOD_M$.

single-channel optical depths (AOD_S) for the shorter wavelength are clustered slightly above the line, while those for 1632 nm are clustered more around it, but the scatter is somewhat larger in the latter case. There is some indication that as the AOD increases the deviation from the one-to-one line increases, and at higher AOD the single-channel algorithm underestimates the AOD relative to the multichannel value (AOD_M). The deviation is especially noticeable for the Aqua 2119-nm channel. The Pearson linear correlation coefficients (r) indicate strong correlation between the AODs. Note that these correlations are weaker at the longer wavelengths; the decrease in correlation is the result of the increased scatter in the data at these wavelengths. The Pearson coefficients are likely to be inflated because of the outliers with large optical depths. As a more robust and resistant alternative to the Pearson correlation, Kendall's rank correlation was also calculated. The Kendall correlation indicates a weaker but still significant correlation between the two AODs. These correlations at the shorter wavelengths are 0.83 (instead of 0.97) for both Terra and Aqua. At the longer wavelengths they are 0.74 (instead of 0.94) for Terra and 0.83 (instead of 0.96) for Aqua. All of these correlations are highly significant as indicated by their two-sided significance values that were essentially zero.

[21] To further quantify the level of agreement between the two AOD retrievals the data were fitted with straight lines. Linear fits were chosen since ideally the two retrievals should agree. In addition to the standard linear fit an orthogonal fit was also calculated. In the orthogonal fit an attempt was made to characterize the errors in both the single-channel and multichannel AOD retrievals. The multichannel retrieval assumed the error $\sigma_M = \pm 0.03 \pm 0.05\tau$ [Remer et al., 2005]. The error in the single-channel retrieval was estimated to be at least as large as that in the multichannel retrieval. However, because the single-channel algorithm uses a fixed aerosol model, the overall error is

expected to be larger than σ_M . Zhao et al. [2004, 2005a, 2005b] found a maximum AOD error of about 40% on regional scales due to the use of a fixed aerosol model. This value was adopted for estimating the combined single-channel error $\sigma_S = \sigma_M/(1-0.4)$. Figure 2 shows the two fitted lines and the corresponding fit parameters. The orthogonal fits returned a q value of one (1.0) indicating a significant fit. The fit parameters along with their standard errors are summarized in Table 1. It is noted that when errors in both retrievals are accounted for (orthogonal fit) the offset is smaller and the slope is closer to unity. Note the generally degraded fit (agreement) as the wavelengths increases.

[22] The overestimation at low AOD and underestimation at high AOD by the single-channel algorithm is also evident from the histograms shown in Figure 3. The distribution of single-channel 644-nm AODs and 1632-nm Terra AODs are slightly skewed relative to the multichannel distribution. The deviation for the Aqua 2119-nm AOD is larger and it is in the direction of smaller AODs.

[23] Summary statistics of the histograms are shown in Tables 2 and 3. Table 2 displays the mean, minimum, and maximum of optical depth values. We note that the small negative AOD from the single-channel retrieval from Terra at 644-nm is the result of the top of atmosphere reflectance being out of range of the reflectances in the LUT. When this happens the algorithm extrapolates, and when the reflectance is smaller than the smallest value in the LUT the retrieved AOD will be negative. This usually happens when the Rayleigh optical depth and/or the surface reflectance assumed in the LUT are too high compared to the actual values, or when the TOA reflectance is too low (e.g., due to calibration errors). The negative AOD is of course unphysical, but it is reported for statistical purposes. It also provides an indication of potential problems.

[24] The total number (N) of retrievals, the mean difference ($MD = \frac{1}{N} \sum (\tau_{S,i} - \tau_{M,i})$), the mean absolute difference ($MAD = \frac{1}{N} \sum |\tau_{S,i} - \tau_{M,i}|$) and the root-mean-square difference ($RMSD = \sqrt{\frac{1}{N} \sum (\tau_{S,i} - \tau_{M,i})^2}$) are shown in Table 3.

MD is calculated primarily because it was also used in the previous comparisons by Ignatov et al. [2005, 2006] and Zhao et al. [2005a, 2005b] and their results are compared with MD in the current study. MAD is calculated to provide a more robust estimate of the difference, although the RMSD also provides a measure of the pairwise differences.

[25] MDs for Terra are small for both channels; they are 0.004 and 0 for 644 nm and 1632 nm, respectively. For Aqua, they are an order of magnitude larger. The mean single-channel AOD is larger than the multichannel one for both Terra and Aqua for both wavelengths, except for the 2119-nm Aqua channel, for which it is smaller than the multichannel one by about 0.02.

[26] It is interesting to note that the 644-nm single-channel mean AOD from Terra and Aqua are quite similar (the difference is only 0.003), while the mean AODs from the multichannel algorithm differ more (the mean AOD from Terra is larger by 0.014 than from Aqua). The Mann-Whitney test performed on single-channel Terra and Aqua AODs also indicated identical median values with a 95.5% confidence. The same test when performed on the multi-

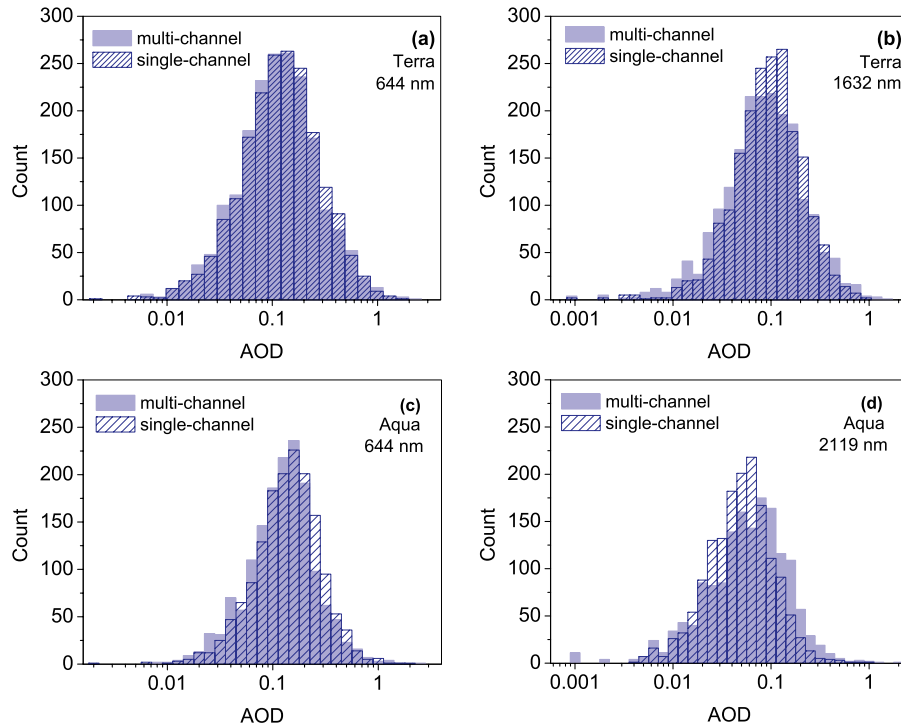


Figure 3. Frequency distribution of single-channel (AOD_S) and multichannel (AOD_M) aerosol optical depths for the short (a, c) and long (b, d) wavelength channels for Terra (Figures 3a and 3b) and Aqua (Figures 3c and 3d).

channel Terra and Aqua AODs suggested significantly different medians at the same confidence level. Whether the Terra and Aqua mean AODs should or should not agree is beyond the scope of this paper. We note, however, that using AERONET data, *Kaufman et al.* [2000] found no significant differences between mean AODs corresponding to the Terra and Aqua observation times. Similarly, *Ichoku et al.* [2005] found no consistent regional trend in the morning-to-afternoon aerosol loading for the regions they examined. We also note that many of these findings, including the similarity of the mean single-channel 644-nm AOD from Terra and Aqua, were also observed by *Ignatov et al.* [2005] who used a different time period and different data set.

[27] The MAD and RMSD values in Table 3 suggest that the small MD values may be the results of cancellations. The MAD values are 0.022–0.025, and almost independent of channel and platform. The RMSD are very similar for both wavelengths and both satellite platforms (0.034–0.038), except for the Aqua 2119-nm AOD where it is 0.053.

Table 2. Mean, Minimum, and Maximum of Single-Channel and Multichannel AODs for Terra and Aqua

Wavelength (nm)	Data	Mean	Min	Max
<i>Terra</i>				
644	AOD_S	0.177	0.005	1.230
	AOD_M	0.173	0.012	1.646
1632	AOD_S	0.094	0.001	0.671
	AOD_M	0.094	0.001	0.950
<i>Aqua</i>				
644	AOD_S	0.174	−0.002	2.010
	AOD_M	0.159	0.008	2.471
2119	AOD_S	0.065	0.004	1.101
	AOD_M	0.085	0.000	2.199

[28] Table 3 also lists the MD, MAD, RMSD and N from the 50-km retrievals. Even though there are about twice as many retrievals in the 50-km samples, no significant differences between the AODs are apparent at these two spatial scales. The statistics are quite similar; the 50-km results exhibit only a slightly reduced/increased MD for the short/long wavelength in comparison with the 10-km values. The 50-km MAD and RMSD values are somewhat larger than their 10-km counterparts; the largest scatter occurs for Aqua at 2119 nm, where the RMSD is as large as 0.069. Because of the similarities between the 10-km and 50-km results, in what follows, only the 10-km results will be presented and discussed.

[29] The single-channel and multichannel retrievals represent two “measurements” of the true AOD that existed when the MODIS observations were taken. Ideally, the retrievals (and the true AOD) should be characterized by the same probability distribution function (pdf). This ex-

Table 3. Mean, Mean Absolute, and Root-Mean-Square AOD Differences for the Two Spatial Domains in MAPSS^a

Resolution (nm)	10-km				50-km			
	MD	MAD	RMSD	N	MD	MAD	RMSD	N
<i>Terra</i>								
644	0.004	0.022	0.035	1938	0.002	0.026	0.050	3944
1632	0.000	0.022	0.034	1938	−0.005	0.027	0.055	3944
<i>Aqua</i>								
644	0.015	0.024	0.038	1569	0.014	0.028	0.049	3217
2119	−0.020	0.025	0.053	1569	−0.029	0.034	0.069	3217

^aN, number of data; MAPSS, Moderate Resolution Imaging Spectroradiometer (MODIS) Atmosphere Parameters Subset Statistics; MD, mean (single channel minus multichannel) difference; MAD, mean absolute difference; and RMSD, root-mean-square difference.

Table 4. Results of the Kolmogorov-Smirnov test^a

Platform	Wavelength (nm)	KS statistic	Probability
Terra	644	0.041	0.075
	1632	0.076	0.000
Aqua	644	0.085	0.000
	2119	0.142	0.000

^aKolmogorov-Smirnov (KS) statistics and their probability are shown for the short and long wavelengths and for Terra and Aqua.

pectation can be used to quantify the differences in the two retrievals on the basis of their pdf's by answering the question of whether the two samples represented by the single-channel and multichannel retrievals are drawn from the same population. We use the nonparametric test of Kolmogorov-Smirnov (KS) statistics as an appropriate and widely applied metric that measures the difference between the cumulative distribution functions (CDF). The results of the KS test are shown in Table 4. For the Terra 644-nm AOD the KS statistic is 0.041 with a probability of 0.075. On the basis of this probability, the two distributions of the 644-nm Terra AODs can be consistent, at the 5% significance level, with a single distribution function; that is, we cannot rule out the possibility that the two distributions are from the same population. However, for the 1632-nm Terra AOD and for Aqua at both wavelengths the KS statistics are at least twice as large with a probability value of (essentially) zero. These probabilities suggest that the single-channel and multichannel AODs do not represent the same population at the 5% level for the long-wavelength Terra and the Aqua AODs.

[30] The retrieved AODs are expected to follow a lognormal distribution [O'Neill *et al.*, 2000]. This expectation, again, is used to characterize the similarities or differences between the single-channel and multichannel retrievals. Parameters of the lognormal distributions (location and scale) were obtained from the retrieved AODs using least squares estimation. Pointwise 95% confidence intervals (CI) were also calculated. These lines are plotted, separately for the single-channel and multichannel retrievals, on a probability plot, which has the natural logarithm of the AOD on the x axis and the value returned for the probability by the inverse CDF for the standard normal distribution on the y axis (Figure 4). In this plot, the fitted distribution lines form straight lines. Similarly, to the extent the lognormal distributions fit the data, the plotted points of the estimated CDF of retrieved AODs also form a straight line in this plot. Although the majority of points fall along the respective fitted CDF, there are several points in the tails that are outside of the confidence bands. The plots indicate that for Terra there are more data associated with small and large AOD values than the lognormal distribution would imply. For Aqua, there are fewer data in the right tail (large AOD) than one would expect on the basis of the fitted distributions. Qualitatively, the estimated CDFs for Terra at 644 nm are

only a little different from each other; also, the lines of fitted CDFs almost overlap. This difference is larger for Aqua for the same wavelength. Moreover, the difference between the two estimated CDFs increases with wavelength.

[31] To quantify how well the single-channel and multichannel AODs fit the lognormal distribution the Anderson-Darling (AD) statistic and associated probability (P) are calculated. These values are also shown in Figure 4. The large AD and small P values indicate that none of the AODs fit particularly well the lognormal distribution at the 5% level. The AD increases with wavelength for both retrievals, and they are the largest for Aqua. It is interesting that the single-channel retrieval from Aqua seems to better fit the lognormal distribution than the multichannel retrieval. For Terra, the opposite seems to be the case, although the differences in the AD statistics are not as large as those for Aqua.

[32] In an attempt to explain the observed differences between the single-channel and multichannel retrievals at low AOD values, where nonaerosol related effects are expected to dominate, reflectances directly calculated from the multichannel (MODIS) and single-channel lookup tables (LUT) with no aerosol were compared. (For this, the single-channel LUT was constructed for the same angular bins as used in the MODIS LUT.) The difference between these reflectances represents the difference due to all nonaerosol components of the algorithms including the surface reflectance, molecular scattering and the radiative transfer model used. For all three wavelengths, the single-channel reflectances for zero AOD were found smaller than the multichannel TOA reflectances (Table 5). The reflectance differences ($\Delta\rho$) were approximately converted to AOD differences ($\Delta\tau$) using the linearized single-scattering approximation as $\Delta\tau = -(4\mu_v\mu_s/\omega P)\Delta\rho$, where μ_v , μ_s , ω and P are the cosines of view and solar zenith angles, aerosol single-scattering albedo and phase function from the single-channel algorithm, respectively. The negative sign in the equation accounts for the fact that a deficit in the modeled reflectance is accounted for an increase of AOD in the retrieval process.

[33] These expected AOD differences can be related to the offsets in the linear fits in Table 1 which by definition are the single-channel AODs at the time when the multichannel MODIS algorithm detected no aerosol. Both these AOD differences and the offsets from the least absolute deviation fit are included in Table 5. The offsets from the least absolute deviation fit were selected for this comparison since this fit is less sensitive to outliers. (We note that the offsets from the orthogonal fit are also comparable to these when the standard errors are included.) The values reported in Table 5 are the averages over the geometries satisfying the retrieval domain adopted in both retrievals (solar zenith angle $<70^\circ$; view zenith angle $<60^\circ$; relative azimuth angle $>90^\circ$ and glint angle $>40^\circ$). A comparison of the AOD

Figure 4. Empirical (symbols) and fitted (lines) cumulative distribution functions of Terra (a, b) and Aqua (c, d) short (Figures 4a and 4c) and long (Figures 4b and 4d) wavelength AODs. In the fitting a lognormal distribution was assumed. The fit parameters of the distribution (Loc and Scale), as well as the Anderson-Darling (AD) statistic and its probability (P), are shown in the box. Three lines are shown for each algorithm: the middle one is the fitted cumulative distribution function (CDF) of the lognormal distribution, while the outer ones are the pointwise (95%) confidence intervals. See section 3 for further details.

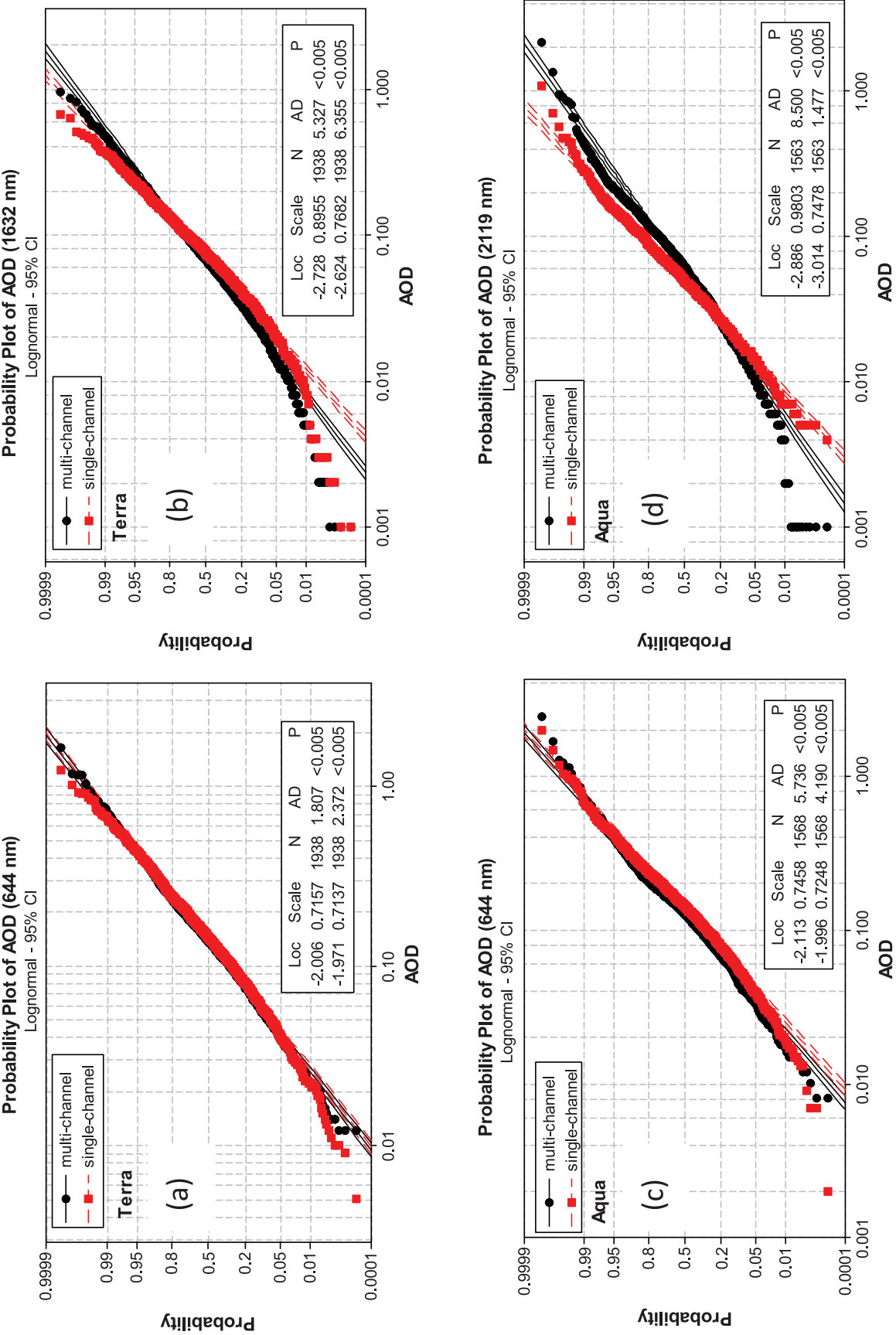


Figure 4

Table 5. Average Difference of Single-Channel and Multichannel Reflectances Predicted by the LUT in the Retrievals for Zero Aerosol Optical Depth, Corresponding AOD Difference, and Offsets of the Least Absolute Deviation Linear Regressions in Table 1^a

Wavelength (nm)	$\Delta\rho$	$\Delta\tau$	Offset	
			Terra	Aqua
644	−8.6E−4	0.009	0.008	0.013
1632	−3.8E−4	0.006	0.018	
2119	−2.8E−4	0.004		0.012

^aLUT, lookup tables; $\Delta\rho$, reflectance difference; $\Delta\tau$, AOD difference.

differences and offsets suggests that nonaerosol (radiative transfer and surface reflectance) related differences are partially responsible for the differences between the single-channel and multichannel AOD values at low AOD. However, these AOD differences are not large enough to fully explain the offsets at longer wavelengths.

[34] The single-channel LUT was also calculated with the same wind speed of 6 m/s as used in the multichannel algorithm. With this LUT the differences between single-channel and multichannel reflectances for zero aerosol optical depth became positive for all three channels (4.7E−4, 1.5E−4 and 1.9E−4) and led to an underestimation of AOD by the single-channel algorithm (by 0.011, 0.003 and 0.003, respectively for the 644-, 1632 and 2119-nm wavelengths) for very small multichannel AOD. This demonstrates that differences in the calculated surface reflectances contribute strongly to the AOD differences at these small values. *Kahn et al.* [2007] reached a similar conclusion by analyzing MODIS and MISR AOD retrievals. They found that the MISR-retrieved AOD was biased high when the actual value of the water-leaving reflectance was higher than assumed (zero), and the MODIS-retrieved AOD was biased low when the actual wind speed was lower than the assumed 6-m/s value. They noted that the MISR midvisible AOD over water was 0.02–0.03 higher than MODIS, due, most likely, to assumed wind speed and calibration differences.

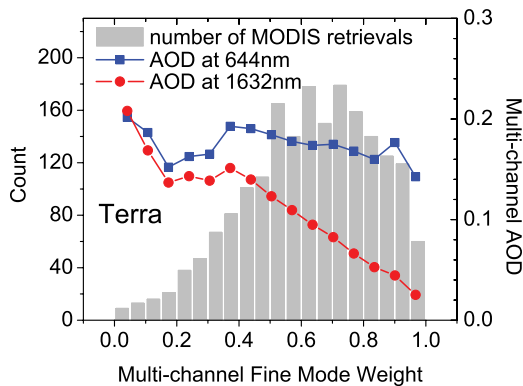


Figure 5. Multichannel AOD as a function of fine-mode weight (FMW) for Terra at the two wavelengths used in the study. The number of multichannel (MODIS) retrievals is also displayed. Most of the particles reported by the multichannel algorithm at the sites selected in this study are small in size (FMW = 0.5–0.9).

[35] It was shown in Figure 2 that the single-channel AODs tend to develop a low bias relative to the multichannel ones as AOD increases. This tendency is more noticeable as the wavelength increases. Since differences in molecular and surface contributions are expected to be less significant for large AOD, the difference in the aerosol models applied by the algorithms is used to try to explain the observed features. We use the multichannel fine-mode weight (FMW) as a proxy for aerosol type. The use of FMW to distinguish between aerosol types was also recommended by *Zhang and Reid* [2006]. They noted that FMW “could be used as a self-consistent parameter in distinguishing aerosol microphysical properties”; and attributed a FMW less than 0.5 to sea salt and dust and a FMW greater than 0.7 to fine pollution and smoke.

[36] Figure 5 plots the multichannel AOD as a function of fine-mode weight (FMW) for Terra at the two wavelengths used in this study. (A similar picture was obtained for Aqua.) It shows that, for the sites selected in this study, larger AODs tend to be associated with larger particles (smaller FMW), while smaller AODs tend to correspond to smaller particles (larger FMW). The single-channel algorithm assumes a fixed average aerosol model. Any deviation from this model is expected to lead to some degree of underestimation or overestimation of AOD in the single-channel model. This trend is shown in Figure 6 that plots

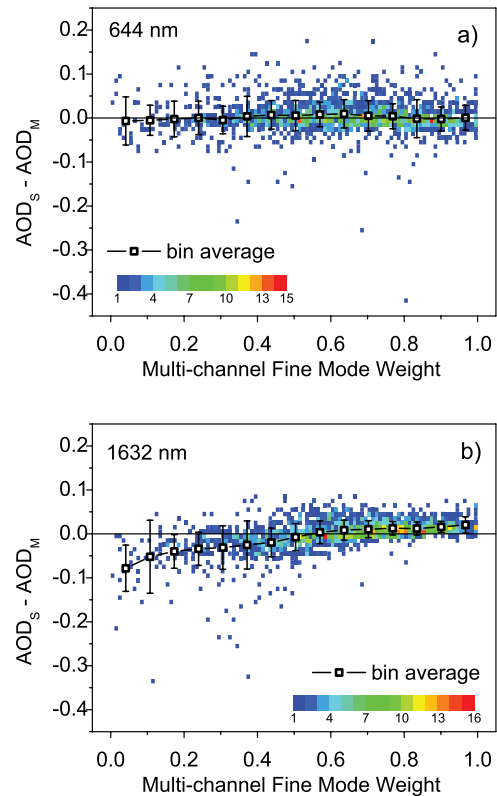


Figure 6. AOD difference ($AOD_S - AOD_M$) as a function of multichannel fine-mode weight for Terra at (a) 644 nm and (b) 1632 nm. The scale represents the number of AOD values. The square symbols are the bin-averaged AOD differences, and the vertical bars show the standard deviations.

Table 6. Mean, Mean Absolute, and Root-Mean-Square AOD Differences for Three Ranges of the Multichannel Fine-Mode Weight^a

FMW	0.0–0.3	0.3–0.6	0.6–1.0
<i>Terra 644 nm</i>			
MD	−0.002	0.005	0.004
RMSD	0.040	0.034	0.034
MAD	0.030	0.022	0.021
N	146	661	1131
<i>Terra 1632 nm</i>			
MD	−0.042	−0.011	0.013
RMSD	0.067	0.040	0.022
MAD	0.047	0.026	0.016
N	146	661	1131
<i>Aqua 644 nm</i>			
MD	0.013	0.016	0.014
RMSD	0.054	0.037	0.035
MAD	0.033	0.025	0.022
N	185	624	760
<i>Aqua 2119 nm</i>			
MD	−0.054	−0.030	−0.004
RMSD	0.108	0.057	0.019
MAD	0.055	0.033	0.011
N	185	624	760

^aMD, mean difference; MAD, mean absolute difference; RMSD, root-mean-square difference; and FMW, fine-mode weight.

the $AOD_S - AOD_M$ difference as a function of the multichannel fine-mode weight for Terra. (The general pattern for Aqua is similar and therefore it is not shown.) The dependence on FMW is negligible at 644 nm. At the longer wavelength and below FMW of ~ 0.5 , however, the AOD difference steadily increases as the FMW decreases; that is when the contribution of coarse mode according to the multichannel algorithm increases. Above FMW of ~ 0.5 the difference is small, and the best agreement between single-channel and multichannel AOD occurs for FMW of ~ 0.6 . Since for most retrieval the FMW is 0.5–0.9, as indicated in Figure 6 by the scale that represents the number of occurrence of particular FMW values, the $AOD_S - AOD_M$ difference is small on the average.

[37] The three differences (MD, MAD, and RMSD) were also calculated for three ranges of the multichannel fine-mode weight: $FMW \leq 0.3$ (“large”), $0.3 < FMW < 0.6$ (“medium”), and $FMW \geq 0.6$ (“small”). The results are shown in Table 6. For Terra, there are about twice as many multichannel retrievals indicating small particles than medium size particles, and about eight times as many as the ones with large particles. For Aqua, the number of retrievals with small and medium size particles is about the same; and it is about four times larger than the number with large particles. The MAD is the smallest for small particles; it is somewhat larger for medium sizes, and it is the largest for large particles. The RMSD is also the largest (0.04–0.11) for large particles. MD varies in sign and magnitude with particle size and with wavelength. For example, the mean AOD from the single-channel retrieval is smaller than that from the multichannel retrieval for all three particle size groups at the Aqua 2119-nm channel; the difference progressively decreases as the particle size decreases.

[38] Dependence of the AOD differences on the observing geometry was also analyzed, and a slight dependence on the scattering angle was found. This is shown in Figure 7

for Terra where the single-channel minus multichannel AOD difference is plotted as a function of the scattering angle for the wavelengths of 644 nm and 1632 nm. For the 644-nm channel and between scattering angles of 130 and 160 degrees, the AOD difference does not change with scattering angle. However, the single-channel AOD is smaller than the multichannel one at the lower end of the scattering angle range and it is larger at the upper end. The pattern for the 1632 nm channel is largely similar, except at the upper end of the scattering angle range where the AOD difference becomes negative again. According to the multichannel retrieval, for the sites used in this study, larger (coarse mode) particles dominate at the extreme scattering angles as shown in Figure 8 that plots the multichannel fine-mode weight as a function of scattering angle. Since, as it was already shown in Figure 6, the largest differences are associated with larger particles it is not surprising to find the largest AOD differences at the extreme scattering angles. (The pattern in Figure 8 is discussed in some more detail in the next section.)

[39] The observation that the largest AOD differences are found at the extreme scattering angles is further demonstrated in Figure 9 that plots the product of phase function and single-scattering albedo of the aerosol models used in the single-channel and multichannel algorithms. For scattering angles below about 130 degrees, the product from the

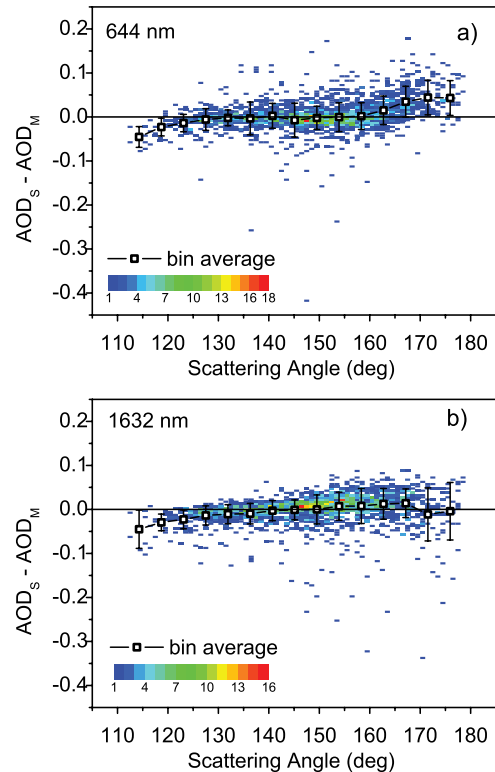


Figure 7. Single-channel (AOD_S) minus multichannel (AOD_M) aerosol optical depth difference as a function of scattering angle for the wavelengths of (a) 644 nm and (b) 1632 nm. The scale represents the number of retrievals; the square symbol is the bin-averaged value of the difference, while the vertical bars denote the standard deviation of differences in the scattering angle bins.

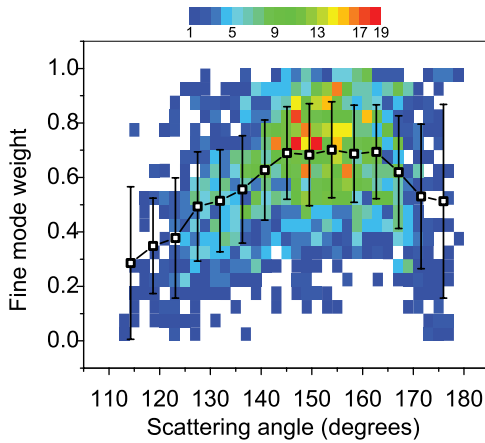


Figure 8. Multichannel-algorithm-derived fine-mode weight as a function of the scattering angle for Terra. The scale represents the number of retrievals; the square symbol is the bin-averaged value of the FMW, while the vertical bars denote the standard deviation of FMW in the scattering angle bins.

single-channel algorithm is generally larger than that of the MODIS coarse modes. This tends to produce a negative AOD difference. At scattering angles larger than about 160 degrees, the product in the single-channel aerosol model is generally smaller than that from most of the multichannel models, and this tends to lead to a larger single-channel AOD.

[40] The scattering angle dependence of AOD difference at 1632 nm (Figure 7b) follows the binned FMW curve (Figure 8). Similar to that at 644 nm, the negative difference at the lower scattering angle end is due to the larger product ωP from the single-channel aerosol model than that from the MODIS coarse modes. However, unlike the 644-nm retrievals, ωP of the single-channel aerosol model is still above that of the three sea salt modes (modes 5, 6, and 7) at the large scattering angle end. This leads to an underestimation of AOD and brings down the AOD difference curve.

4. Summary and Conclusions

[41] Aerosol optical depths (AOD) over 22 oceanic sites were derived from MODIS radiances using the single-channel algorithm employed in the CERES SSF data set. The AODs were derived from the clear reflectances recorded for the Terra and Aqua platforms in the MODIS Atmosphere Parameters Subset Statistics (MAPSS) data. The single-channel AODs were compared to the multichannel AODs available in MAPSS and retrieved by the MODIS group with the standard MODIS over-ocean algorithm from the same clear-sky MAPSS reflectances used in the single-channel retrievals.

[42] A good agreement between the means (MD) of the two AODs was observed in spite of the substantial algorithm differences. It was found that on average, the 644-nm the single-channel AOD was slightly larger (0.004–0.015 or 2–9%) than the multichannel one on both Terra and Aqua. The single-channel and multichannel AODs closely agreed at 1632 nm for Terra, while at 2119 nm for Aqua the

single-channel AOD was smaller by 0.02 (24%) than the multichannel one.

[43] While the mean differences exhibited dependence on wavelength and platform, the mean absolute differences and root-mean-square differences were more consistent from wavelength to wavelength and from platform to platform. MAD and RMSD ranged between 0.022 and 0.025 and 0.035–0.053, respectively. The largest RMSD (0.053) was

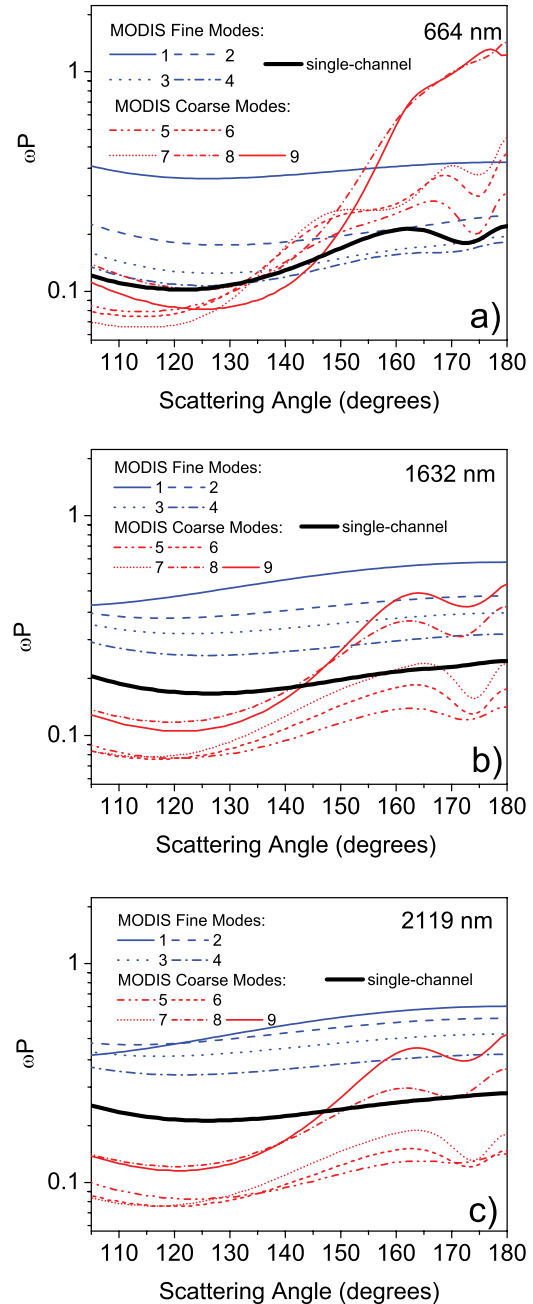


Figure 9. Product of the phase function (P) and the single-scattering albedo (ω) of the aerosol models used in the single-channel and multichannel algorithms. The multichannel (MODIS) algorithm includes nine aerosol models; four fine-mode models (1–4) and five coarse-mode models (5–9). The plots are for (a) 644 nm, (b) 1632 nm, and (c) 2119 nm.

observed at 2119 nm for Aqua. Further statistical tests (KS) indicated that the probability distributions of single-channel and multichannel 644-nm AODs from Terra could be similar at the 5% level. The same test, however, suggested that at the longer wavelength for Terra and at both wavelengths for Aqua the distributions are likely different at the 5% level. These tests in conjunction with the nonzero MAD value suggests that the small MD value at 1632 nm for Terra is largely the result of cancellation between overestimation and underestimation of AOD by the single-channel algorithm with respect to the multichannel AOD.

[44] It was also shown that for small AOD the difference between the ocean surface reflectances used by the single-channel and multichannel algorithms likely significantly contributes to the observed AOD differences. For larger AOD the surface reflectance difference has smaller effect and differences in aerosol models dominate.

[45] The AOD difference exhibited only a weak dependence on scattering angle at the extreme angles. AODs at these angles were found to be associated with large particles, which were not represented well in the fixed aerosol model used by the single-channel algorithm. Thus, the AOD differences observed at these angles were partially attributed to differences in the aerosol models used by the two algorithms. This difference, however, was mitigated in the average AOD by the fact that most aerosol particles encountered were relatively small, and evidently the aerosol model employed in the single-channel algorithm was fairly consistent with the multichannel derived aerosol model for these particle sizes. The mitigation was less effective for Aqua than for Terra as shown by the larger MD values for Aqua. This might be understood considering that the multichannel Aqua retrievals indicated a somewhat coarser aerosol model. The average FMW for Aqua was 0.58 as opposed to the Terra value of 0.63.

[46] Assuming that the expected AOD uncertainty estimate of $\Delta\tau = \pm 0.03 \pm 0.05 \tau$ over ocean for MODIS designated at 550 nm [Remer *et al.*, 2005] is valid for other wavelengths as well, the range of AOD for the multichannel mean values shown in Table 2 are (0.136, 0.214) and (0.061, 0.130) for Terra for the 644- and 1632-nm channels, respectively. The single-channel averages of 0.177 and 0.094 at these wavelengths are well within this range. Similarly, the single-channel 644- and 2119-nm AOD averages of 0.174 and 0.065 for Aqua are within the multichannel ranges of (0.123, 0.200) and (0.052, 0.121).

[47] For the sites studied, the multichannel derived fine-mode weights are ~ 0.7 for the dominant scattering angles of 140–160 degrees (Figure 8). FMW decreases progressively as the scattering angle approaches the extreme values in the observational range (110 and 180 degrees). This scattering angle dependence of the multichannel retrieved FMW is not anticipated since the algorithm is expected to perform uniformly over the entire range of retrieval conditions. We note, however, that the feature depicted in Figure 8 does not necessarily mean the multichannel FMW has a scattering angle dependent bias. First, the number of retrievals performed at the extreme scattering angles is an order of magnitude smaller than those between 130 and 160 degrees. Second, the standard deviation of FMW is also very large at the extreme angles. Third, not all sites are observed at the extreme scattering angles; for

example only half of the sites are “seen” at scattering angles in the range of 110–130 degrees. These sites include (in the notations in Figure 1) Bermuda Ocean, E Mediterranean, E Brazil, Japan Ocean, NE Pacific, NW Pacific, SE Pacific, North Atlantic, SE Africa, South India and West Europe. However, it is not immediately obvious if all these sites are indeed associated with large aerosol particles. More in depth investigation is needed that is beyond the scope of the current study.

[48] The results presented in the current work confirm the findings of Ignatov *et al.* [2005, 2006] and indicate that algorithm differences may account for some (but likely small fraction) of the differences observed in those works. For a more definite conclusion, one should repeat the work presented here with AOD data from CERES-SSF grids matched with the MAPSS sites used in the current study.

[49] The results also reemphasize the usefulness of single-channel aerosol retrievals made in the past from AVHRR. The close agreement of MDs from the two retrievals indicates the need for more comprehensive analyses of the information content of multispectral aerosol retrievals relative to the simpler retrieval techniques. Results of such research would be instrumental for establishing the most accurate yet simple and robust retrieval techniques, ranking different graceful degradation options, and ultimately building linkages between the heritage and newer sensors and products.

[50] **Acknowledgments.** We thank L. Remer, C. Ichoku, and R. Levy of NASA/GSFC for help with the MAPSS data and with the MODIS algorithm. Helpful discussions on the subject with members of the CERES Science Team (PI: B. Wielicki and N. Loeb of NASA/LaRC) are also acknowledged. Partial funding for the work was provided by the Integrated Program Office (S. Mango and K. St. Germain, managers). We also appreciate the thoughtful and very thorough reviews of two anonymous reviewers whose comments helped to improve the paper. Although this work was internally reviewed, the views, opinions, and findings contained in it are those of the authors and should not be construed as an official NOAA or U.S. Government position, policy, or decision.

References

- Ahmad, Z., and R. Fraser (1982), An iterative radiative transfer code for ocean-atmosphere system, *J. Atmos. Sci.*, 39, 656–665, doi:10.1175/1520-0469(1982)039<0656:AIRTCF>2.0.CO;2.
- Deuze, J. L., P. Goloub, M. Herman, A. Marchand, G. Perry, S. Susana, and D. Tanré (2000), Estimate of the aerosol properties over the ocean with POLDER, *J. Geophys. Res.*, 105(D12), 15,329–15,346, doi:10.1029/2000JD900148.
- Diner, D. J., et al. (1998), Multi-angle Imaging Spectroradiometer (MISR): Instrument description and experiment overview, *IEEE Trans. Geosci. Remote Sens.*, 36(4), 1072–1087, doi:10.1109/36.700992.
- Geier, E. B., R. N. Green, D. P. Kratz, P. Minnis, W. F. Miller, S. K. Nolan, and C. B. Franklin (2003), CERES data management system: Single Satellite Footprint TOA/surface fluxes and clouds (SSF) collection document, release 2, version 1, 212 pp. and appendixes NASA Langley Res. Cent., Hampton, Va. (Available at http://asd-www.larc.nasa.gov/ceres/collect_guide/SSF_CG.pdf).
- Higurashi, A., and T. Nakajima (1999), Development of a two-channel aerosol retrieval algorithm on a global scale using NOAA AVHRR, *J. Atmos. Sci.*, 56(7), 924–941, doi:10.1175/1520-0469(1999)056<0924:DOATCA>2.0.CO;2.
- Ichoku, C., D. A. Chu, S. Mattoo, Y. J. Kaufman, L. A. Remer, D. Tanré, I. Slutsker, and B. N. Holben (2002), A spatio-temporal approach for global validation and analysis of MODIS aerosol products, *Geophys. Res. Lett.*, 29(12), 8006, doi:10.1029/2001GL013206.
- Ichoku, C., L. A. Remer, and T. F. Eck (2005), Quantitative evaluation and intercomparison of morning and afternoon Moderate Resolution Imaging Spectroradiometer (MODIS) aerosol measurements from Terra and Aqua, *J. Geophys. Res.*, 110, D10S03, doi:10.1029/2004JD004987.
- Ignatov, A., J. Sapper, S. Cox, I. Laszlo, N. R. Nalli, and K. B. Kidwell (2004), Operational aerosol observations (AEROS) from AVHRR/3 on

- board NOAA-KLM satellites, *J. Atmos. Oceanic Technol.*, 21(1), 3–26, doi:10.1175/1520-0426(2004)021<0003:OAOAFO>2.0.CO;2.
- Ignatov, A., P. Minnis, N. Loeb, B. Wielicki, W. Miller, S. Sun-Mack, D. Tanré, L. Remer, I. Laszlo, and E. Geier (2005), Two MODIS aerosol products over ocean on the Terra and Aqua CERES SSF datasets, *J. Atmos. Sci.*, 62(4), 1008–1031, doi:10.1175/JAS3383.1.
- Ignatov, A., P. Minnis, W. F. Miller, B. A. Wielicki, and L. Remer (2006), Consistency of global MODIS aerosol optical depths over ocean on Terra and Aqua CERES SSF data sets, *J. Geophys. Res.*, 111, D14202, doi:10.1029/2005JD006645.
- Kahn, R., P. Banerjee, and D. McDonald (2001), Sensitivity of multiangle imaging to natural mixtures of aerosols over ocean, *J. Geophys. Res.*, 106(D16), 18,219–18,238, doi:10.1029/2000JD900497.
- Kahn, R. A., M. J. Garay, D. L. Nelson, K. K. Yau, M. A. Bull, B. J. Gaitley, J. V. Martonchik, and R. C. Levy (2007), Satellite-derived aerosol optical depth over dark water from MISR and MODIS: Comparisons with AERONET and implications for climatological studies, *J. Geophys. Res.*, 112, D18205, doi:10.1029/2006JD008175.
- Kaufman, Y. J., B. N. Holben, D. Tanré, I. Slutsker, A. Smirnov, and T. F. Eck (2000), Will aerosol measurements from Terra and Aqua polar orbiting satellites represent the daily aerosol abundance and properties?, *Geophys. Res. Lett.*, 27(23), 3861–3864, doi:10.1029/2000GL011968.
- Levy, R. C., L. A. Remer, J. V. Martins, Y. J. Kaufman, A. Plana-Fattori, J. Redemann, and B. Wenny (2005), Evaluation of the MODIS aerosol retrievals over ocean and land during CLAMS, *J. Atmos. Sci.*, 62(4), 974–992, doi:10.1175/JAS3391.1.
- Minnis, P., D. Young, B. Wielicki, P. Heck, X. Q. Dong, and L. Stowe (1999), CERES cloud properties derived from multispectral VIRS data, *Proc. SPIE*, 3867, 91–102, doi:10.1117/12.373047.
- Mishchenko, M. I., I. V. Geogdzhayev, B. Cairns, W. B. Rossow, and A. A. Lacis (1999), Aerosol retrievals over the ocean by use of channels 1 and 2 AVHRR data: Sensitivity analysis and preliminary results, *Appl. Opt.*, 38(36), 7325–7341, doi:10.1364/AO.38.007325.
- Mishchenko, M. I., B. Cairns, G. Kopp, C. F. Schueler, B. A. Fafaul, J. E. Hansen, R. J. Hooker, T. Itchikawich, H. B. Maring, and L. D. Travis (2007), Accurate monitoring of terrestrial aerosols and total solar irradiance: Introducing the glory mission, *Bull. Am. Meteorol. Soc.*, 88(5), 677–691, doi:10.1175/BAMS-88-5-677.
- Myhre, G., et al. (2004), Intercomparison of satellite retrieved aerosol optical depth over the ocean, *J. Atmos. Sci.*, 61(5), 499–513, doi:10.1175/1520-0469(2004)061<0499:IOSRAO>2.0.CO;2.
- Myhre, G., et al. (2005), Intercomparison of satellite retrieved aerosol optical depth over ocean during the period September 1997 to December 2000, *Atmos. Chem. Phys.*, 5, 1697–1719.
- O'Neill, N. T., A. Ignatov, B. N. Holben, and T. F. Eck (2000), The log-normal distribution as a reference for reporting aerosol optical depth statistics; Empirical tests using multi-year, multi-site AERONET Sun photometer data, *Geophys. Res. Lett.*, 27(20), 3333–3336, doi:10.1029/2000GL011581.
- Remer, L. A., et al. (2005), The MODIS aerosol algorithm, products, and validation, *J. Atmos. Sci.*, 62(4), 947–973, doi:10.1175/JAS3385.1.
- Stowe, L. L., A. M. Ignatov, and R. R. Singh (1997), Development, validation, and potential enhancements to the second-generation operational aerosol product at the national environmental satellite, data, and information service of the national oceanic and atmospheric administration, *J. Geophys. Res.*, 102(D14), 16,923–16,934, doi:10.1029/96JD02132.
- Stowe, L. L., H. Jacobowitz, G. Ohring, K. R. Knapp, and N. R. Nalli (2002), The Advanced Very High Resolution Radiometer (AVHRR) Pathfinder Atmosphere (PATMOS) climate dataset: Initial analyses and evaluations, *J. Clim.*, 15(11), 1243–1260, doi:10.1175/1520-0442(2002)015<1243:TAVHRR>2.0.CO;2.
- Tanré, D., Y. J. Kaufman, B. N. Holben, B. Chatenet, A. Karnieli, F. Lavenu, L. Blarel, O. Dubovik, L. A. Remer, and A. Smirnov (2001), Climatology of dust aerosol size distribution and optical properties derived from remotely sensed data in the solar spectrum, *J. Geophys. Res.*, 106(D16), 18,205–18,217, doi:10.1029/2000JD900663.
- Vermote, E. F., D. Tanré, J. L. Deuze, M. Herman, and J. J. Morcrette (1997), Second simulation of the satellite signal in the solar spectrum, 6S: An overview, *IEEE Trans. Geosci. Remote Sens.*, 35(3), 675–686, doi:10.1109/36.581987.
- Wielicki, B. A., B. R. Barkstrom, E. F. Harrison, R. B. Lee, G. L. Smith, and J. E. Cooper (1996), Clouds and the Earth's Radiant Energy System (CERES): An Earth observing system experiment, *Bull. Am. Meteorol. Soc.*, 77(5), 853–868, doi:10.1175/1520-0477(1996)077<0853:CATERE>2.0.CO;2.
- Zhang, J. L., and J. S. Reid (2006), MODIS aerosol product analysis for data assimilation: Assessment of over-ocean level 2 aerosol optical thickness retrievals, *J. Geophys. Res.*, 111, D22207, doi:10.1029/2005JD006898.
- Zhao, T. X. P., O. Dubovik, A. Smirnov, B. N. Holben, J. Sapper, C. Pietras, K. J. Voss, and R. Frouin (2004), Regional evaluation of an advanced very high resolution radiometer (AVHRR) two-channel aerosol retrieval algorithm, *J. Geophys. Res.*, 109, D02204, doi:10.1029/2003JD003817.
- Zhao, T. X. P., I. Laszlo, P. Minnis, and L. Remer (2005a), Comparison and analysis of two aerosol retrievals over the ocean in the Terra/Clouds and the Earth's Radiant Energy System: Moderate Resolution Imaging Spectroradiometer single scanner footprint data: 1. Global evaluation, *J. Geophys. Res.*, 110, D21208, doi:10.1029/2005JD005851.
- Zhao, T. X. P., I. Laszlo, P. Minnis, and L. Remer (2005b), Comparison and analysis of two aerosol retrievals over the ocean in the Terra/Clouds and the Earth's Radiant Energy System: Moderate Resolution Imaging Spectroradiometer single scanner footprint data: 2. Regional evaluation, *J. Geophys. Res.*, 110, D21209, doi:10.1029/2005JD005852.

A. Ignatov, Center for Satellite Applications and Research, NOAA/NESDIS, Camp Springs, MD 20746, USA.

I. Laszlo, Center for Satellite Applications and Research, E/RA2, RM7135, NOAA Science Center, NOAA/NESDIS, 5200 Auth Road, Camp Springs, MD 20746, USA. (istvan.laszlo@noaa.gov)

Hongqing Liu, PSGS/QSS Group Incorporated, 4500 Forbes Boulevard, Suite 200, Lanham, MD 20706, USA.